THE JOURNAL OF PHYSICAL CHEMISTRY B

Article

pubs.acs.org/JPCB

Experimental Test of Reflectivity Formulas for Turbid Colloids: Beyond the Fresnel Reflection Amplitudes

Gesuri Morales-Luna,[†] Humberto Contreras-Tello,[‡] Augusto García-Valenzuela,[*,‡] and Rubén G. Barrera[†]

[†]Instituto de Física, Universidad Nacional Autónoma de México, Apartado Postal 20-364, Distrito Federal 01000, México

[‡]Centro de Ciencias Aplicadas y Desarrollo Tecnológico, Universidad Nacional Autónoma de México, Apartado Postal 70-186, Distrito Federal 04510, México

ABSTRACT: We compare light reflectivity measurements as a function of the angle of incidence for an interface between an optical glass and a turbid suspension of small particles, with theoretical predictions for the coherent reflectance calculated with different available theoretical models. The comparisons are made only in a small range of angles of incidence around the critical angle of the interface between the glass and the matrix of the colloidal suspensions. The experimental setup and its calibration procedure are discussed. We considered two Fresnel-based approximations and another two based on a multiple-scattering approach, and we present results for monodisperse latex colloidal suspensions of polymeric spherical particles in water with particle diameters of 120 and 520 nm, polydisperse titanium dioxide (rutile) particles suspensions in water with a most probable diameter of 404 nm, and suspensions of copper particles in water with diameters of 500 nm. The comparisons between experiment and theory are made without fitting any parameters.

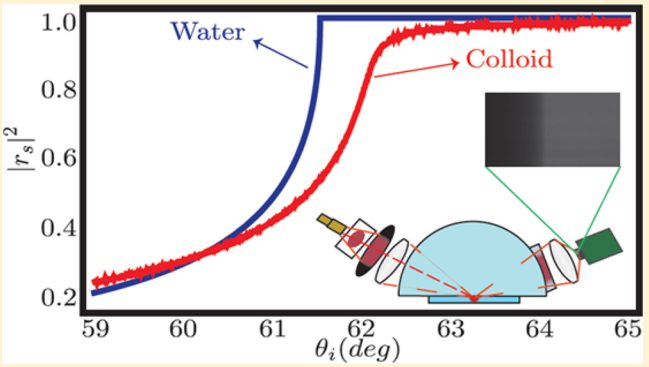

1. INTRODUCTION

The optical properties of colloidal systems have attracted the attention of many researchers[1,2] due to its use as a tool to investigate, with light, the geometric structure and the electromagnetic properties of a wide variety of colloids[3−5] and also because its full understanding leads to the fundamental and still open problem of the interaction of light with a many-body system. Here, the term colloid is used to refer to any two-phase system consisting of a disperse phase embedded within a homogeneous one. The disperse phase will be called colloidal particles, or simply particles or inclusions, while the homogeneous one will be called the matrix. There have been different approaches to formulate the interaction of light with a colloidal system; one has been the straightforward use of multiple-scattering theory,[6] and another one, very fruitful indeed, has been to regard the colloid as a homogeneous effective medium while devising a theory to correlate its effective properties with the set of parameters describing the actual inhomogeneous system.[7] These effective-medium theories have proved to be extremely useful when the size of the particles is very small in comparison with the wavelength of the incident light, giving rise to an active field of research.[7−9] The reason for their usefulness is quite immediate because after having determined the properties of the effective medium, one can deal with the colloidal system as a common homogeneous system in the context of continuous electrodynamics. For example, if one finds an expression for the effective index of refraction, one can use it directly in Snell's law to describe the refractive properties of the actual system.

When the size of the colloidal particles becomes as large or larger than the wavelength of the incident radiation, a new phenomenon takes place; the colloid becomes turbid. This happens because the electromagnetic field scattered by all of the particles and traveling in all different directions is no longer negligible and gives rise to what is known as the diffuse field, and this diffuse field is the physical source of turbidity. If one splits the total electromagnetic field within the colloid in two components, an average component plus a fluctuating component, the latter corresponds to the diffuse field while the former is called the coherent beam or average field. The coherent beam travels in well-defined directions because along these directions, there is always constructive interference of the scattered field, independent of the location of the colloidal particles; in a system with a plane boundary, these directions correspond to the refracted and specularly reflected fields. Thus, by ignoring the presence of the diffuse field, one is able to define an effective medium, related only to the behavior of the coherent beam. Nevertheless, due to scattering, the coherent beam will eventually loose its identity by transferring all of its power to the diffuse field; therefore, the presence of the diffuse

Received: November 4, 2015
Revised: December 25, 2015
Published: January 4, 2016

DOI: 10.1021/acs.jpcb.5b10814
J. Phys. Chem. B 2016, 120, 583−595

field can be taken into account within the framework of an effective-medium theory as an additional "dissipative" process.

There have been attempts to extend the effective-medium theories, so successful in the case of small particles, to larger particles, but these attempts have encountered conceptual problems that have delayed the construction of a rigorous formulation, especially for the case of suspensions with a well-defined flat boundary. First of all, it has been shown[10] that in a boundless system, the effective optical parameters, that is, the effective electrical permittivity ϵ_{eff} and the effective magnetic permeability μ_{eff}, have a spatial nonlocal character, or, equivalently, they are spatially dispersive, that is, they depend not only on the frequency ω but also on the wavevector k of the incident radiation. As a consequence, the dispersion relation $k(\omega)$ for transverse electromagnetic modes for an on-the-average isotropic and homogeneous boundless suspension is given by the solution of $k = \omega\sqrt{\epsilon_{\text{eff}}(k, \omega)\mu_{\text{eff}}(k, \omega)}$. Then, one can define a frequency-dependent index of refraction $n_{\text{eff}}(\omega)$ as $n_{\text{eff}}(\omega) = [ck(\omega)]/\omega$, where c is the speed of light. It was also shown[10] that $n_{\text{eff}}(\omega)$ obtained this way can be used freely and rigorously in Snell's law, giving rise to several applications using only refraction measurements.[11,12] Nevertheless, when $n_{\text{eff}}(\omega)$ was used to calculate reflection amplitudes from a turbid suspension, using Fresnel's formulas, inconsistencies were found.[13,14] This is so because in this case, the approximate validity of Fresnel's formulas and effective optical parameters deteriorate as the size and scattering efficiency of the colloidal particles increases, and they eventually breakdown. In such cases, a different approach going beyond effective-medium theory has to be devised. This has been recently done in refs 15−17. We will refer to formulas for the coherent reflectance of light derived explicitly from the multiple-scattering formalism[15,16] as the coherent scattering model (CSM), whereas the corresponding expressions derived in refs 18 and 19 are called extended Fresnel's formulas. At a flat interface with a colloidal suspension of particles, the contribution to the specularly reflected coherent field coming from the colloidal particles can be regarded as the field produced by the constructive interference of the field scattered by all of the particles at a scattering angle given, in the dilute limit, by the angle between the refracted and the reflected beam directions. Because this angle depends on the angle of incidence and the scattering amplitudes of the particles have an angular dependence related to their refractive index (RI), size, and shape, one expects that the dependence of the reflected coherent-field intensity on the angle of incidence will provide information about the optical characteristics of the colloidal particles.

It is not difficult to see that among the different possibilities to measure the reflectance of light from a half-space, the highest sensitivity to the presence of colloidal particles is achieved in an internal reflection configuration, before and around the critical angle as defined by the refractive indices of the incidence medium and the matrix. In fact, some years ago, our research group compared predictions of the CSM and the Fresnel reflection coefficients with an effective RI (then referred to as the isotropic effective medium theory) with experimental reflectance data around the critical angle for a few colloids.[16] The comparison consisted of fitting the theoretical predictions to the experimental data, by adjusting a few parameters used in the theoretical models, to see whether the theories tested were consistent with the experimental results. It was found that the CSM could be adjusted to all of the experimental curves, whereas the Fresnel approximation could not.

The objective of this work is to design a handy experimental setup and to perform reflectance measurements around the critical angle for a few well-characterized colloids with most of the parameters known to a good precision and then compare the recently derived extended Fresnel formulas in ref 19 with experimental data. Here, we also compare the CSM with the experiment and the Fresnel formulas, including in the comparison a simple variation of the Fresnel approximation that takes into account a surface correction due to the finite size of the particles. With these comparisons, we intend to test the validity limits of Fresnel's approximation, of the formulas corresponding to the CSM in ref 15, and of the extended Fresnel's formulas in ref 19. We must emphasize that this work tests the mentioned theories only in an internal reflection configuration and in a limited range of angles of incidence around the critical angle as defined by the matrix. Other ranges of angles of incidence and experiments in an external reflection configuration are left out for future work. We remind the reader that in an external reflection configuration, the RI of the incidence medium is lower than that of the transmission medium, and there is neither a critical angle nor total internal reflection, as can be the case in an internal reflection configuration.

In section 2, we give a brief account of the theoretical formalism, and we discuss also the problems that arise when one tries to extend the concept of an effective nonlocal optical response in the presence of an interface. In section 3, we present the experimental setup describing all of the optical components. In section 4, we explain way we calibrate the system and validate the reflectivity measurements, which we then compare with theoretical predictions in section 5. Finally, in section 6, we present our conclusions.

2. THEORETICAL FORMALISM

In this section, we review briefly the main physical ideas used in the derivation of the formulas for the reflection amplitudes of turbid colloids, whose limits of validity are being tested in this work. We do this so the reader can have an overall picture of the complications that arise in dealing with this problem as well as the precise nature of the approximations being tested. We start by describing the model used in the derivations of the reflection amplitude formulas. Then, we recall the formula for the bulk effective RI of a dilute colloidal suspension and the commonly used Fresnel's approximation to the coherent reflectance, based on this effective RI. Then, we summarize the formulas for the coherent reflectance within the CSM reported in ref 15 and then the ones for the so-called heuristic approximation (HA) of the extended Fresnel's formulas derived in ref 19. We first present these approximations considering that the incidence medium is the same as the matrix of the half-space of randomly placed particles, as depicted in Figure 1. Then, we show how to construct the corresponding approximations in case the incidence medium has a different RI than the matrix of the colloid by using a well-known reflection amplitude composition formula. Finally, we show how to extend the considered approximations to polydisperse colloidal systems.

2.1. Monodisperse Model. We regard the bulk colloidal system as a large collection of $N \gg 1$ randomly located identical spheres of radius a and electric permittivity $\epsilon_s(\omega)$, all immersed within a boundless homogeneous matrix with electric

DOI: 10.1021/acs.jpcb.5b10814
J. Phys. Chem. B 2016, 120, 583−595

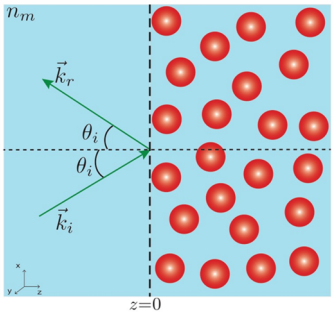

Figure 1. Illustration of a half-space of randomly placed particles, considering that the incidence medium is the same as the one where the particles are immersed. Here $\vec{k}_i$ and $\vec{k}_r$ are the wavevectors of the incidence and the reflected plane waves, respectively, and θ_i is the angle of incidence.

permittivity $\epsilon_m(\omega)$. Here, ω is the (angular) frequency of an electromagnetic plane wave that excites the colloidal system. The system will be called homogeneous "on the average" if the probability of finding the center of a sphere is the same at any point in space. Now, in order to build an interface in this system, there are many different ways to do it. Here, we choose a plane, say the $z = 0$ plane in a Cartesian coordinate system, such that the probability of finding the center of a sphere within dV for $z > a$ is constant and equal to dV/V and is zero for $z < a$, where dV is the differential of volume and V is the total volume of the system. The reason for this choice will be discussed later. On one hand, the plane $z = 0$ is called the nominal surface because although there is zero probability of finding the center of a sphere for $0 < z < a$, the edge of a sphere could actually reach the plane $z = 0$. On the other hand, the plane $z = a$ will be called the probability interface. Note that in this model of the interface, the index of refraction of the incidence medium ($z < 0$) is the same as the one of the colloidal matrix.

Now, to define the reflection amplitudes at the nominal surface, one excites the system with an incident plane wave with wavevector $\vec{k}$ and frequency ω coming from $z < 0$, and the reflection amplitudes r are defined as the quotient of the amplitudes of the electric field of the reflected wave over the amplitude of the incident one. They are denoted either r_s or r_p depending on whether the polarization of the incident plane wave is either perpendicular or parallel to the plane of incidence. Finally, we recall that turbidity appears when the size of the inclusions is on the order of the wavelength of the incident radiation because then scattering is prominent.

2.2. Effective Refractive Index and Fresnel's Approximation. Using the model described above, the bulk effective RI felt by the coherent wave as it travels through a boundless colloidal medium has been derived by several authors over the years (see, for instance, refs 15 and 20−22). One has, for example, the rather simple expression given by Foldy−Lax[20−22]

$$n_{\text{eff}} = \sqrt{1 + 2i\gamma S(0)} \tag{1}$$

Here, $\gamma = 3f/2x^3$, where $x = k_o n_m a$, is called the size parameter, n_m is the RI of the medium, $k_o = 2\pi/\lambda$ is the wavenumber, λ is the wavelength of the incident radiation, a and f denote the radius and volume-filling fraction of the spherical particles, respectively, while $S(0)$ is the forward-scattering amplitude of an isolated sphere, as defined in ref 8. If $f \ll 1$ (dilute limit), the above formula, usually called the Foldy−Lax formula, simplifies and yields the so-called van de Hulst's effective RI,[7] given by

$$n_{\text{eff}} = 1 + i\gamma S(0) \tag{2}$$

Now, we introduce the simplest approximation for the calculation of the reflection amplitudes that does not require any assumption whatsoever about the structure of the interface. One only assumes that the half-space ($z > 0$) where the colloids resides is occupied by an effective medium with an effective bulk RI n_{eff} given by either eq 1 or 2. Then, if one assumes that there is no magnetic response of the colloid, one can use n_{eff} directly in the Fresnel's reflection formulas, given for s and p polarization by

$$r_s = \frac{k_z^i - k_z^{\text{eff}}}{k_z^i + k_z^{\text{eff}}} \tag{3}$$

$$r_p = \frac{\epsilon_i k_z^{\text{eff}} - \epsilon_{\text{eff}} k_z^i}{\epsilon_{\text{eff}} k_z^i + \epsilon_i k_z^{\text{eff}}} \tag{4}$$

where $\epsilon_i = (n_i)^{1/2}$ and $\epsilon_{\text{eff}} = (n_{\text{eff}})^{1/2}$ are the electric permittivity of the incidence and transmitted media, respectively, and k_z^i and k_z^{eff} are the z-components of the incident and transmitted wavevector. k_z^{eff} can be expressed as

$$k_z^{\text{eff}} = k_o n_i \sqrt{n_{\text{eff}}^2 - n_i^2 \sin^2(\theta_i)} \tag{5}$$

where θ_i is the angle of incidence at the first medium. We will call this approximation the two-media Fresnel's approximation (2MF), and it is the most straightforward and commonly used approximation. One might wonder why we call this an approximation. The reason is because one is assuming without any justification (i) that the colloidal system with nonmagnetic inclusions has no magnetic response and (ii) that in the presence of an interface, it is still valid to use the bulk effective index of refraction in Fresnel's formulas. We will see below that both of these assumptions become invalid as the size of the inclusions becomes on the order of the wavelength of incidence radiation.

2.3. Coherent Scattering Model. In the CSM, it becomes necessary to use the probabilistic model of the interface described above. One starts by dividing the half-space occupied by the colloid into equally spaced slabs of width d, each one containing a given number of (centers of) spherical particles,[15] as shown in Figure 2. The calculation procedure relies on first obtaining the coherent reflection and transmission amplitudes of a single layer. This is done by exciting the layer with an incident plane wave and then calculating the scattered electric field of all of the particles in the slab on a plane-wave basis.

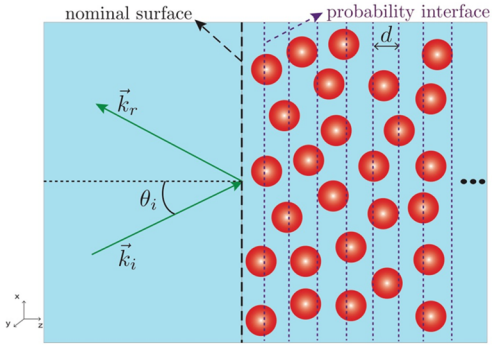

Figure 2. Illustration of a half-space of a random distribution of particles divided in equally spaced slabs. The incidence medium and the matrix are the same medium.

DOI: 10.1021/acs.jpcb.5b10814
J. Phys. Chem. B 2016, 120, 583−595

Because one is interested only in the coherent component of the scattered field, one performs a configurational average of the scattered electric field over a slab of width d. In the averaging procedure, one further assumes that the centers of the particles are uncorrelated and that the probability of finding a particle with its center within d^3r is uniform and equal to d^3r/V, where V is the volume of the slab. As a consequence, one gets explicit expressions for the reflection and transmission amplitudes in terms of the forward-scattering amplitude $S(0)$ and the elements of the scattering matrix $S_j(\pi - 2\theta_i)$, where $j = 1$ corresponds to s polarization while $j = 2$ corresponds to p polarization. Here, θ_i is the angle of incidence, $\pi - 2\theta_i$ is the direction of the reflected wave, and $S(0) = S_1(0) = S_2(0)$. Now, the coherent reflection from a half-space can be obtained by calculating the reflection amplitude of a semi-infinite pile of thin slabs of width d. If the slabs are thin enough ($k_i d \ll 1$), each slab may be regarded as an equivalent 2D sheet. Then, the half-space becomes an infinite stack of equally separated 2D sheets extending to the right of its nominal surface, and this multiple-scattering problem can be solved exactly.[15] We can now recall that the "probability interface" restricts the centers of all of the particles to be on one side of it and places the first of the semi-infinite pile of 2D sheets on this probability interface. Thus, the nominal surface of the colloidal half-space turns out to be located at one particle radius (a) away from the probability interface, as indicated in Figure 2. In this way, we ensure that all of the particles are completely embedded in one half-space starting at the nominal surface.

This calculation yields the following expressions of the reflection amplitudes

$$r_{hs} = \frac{\gamma \frac{S_j(\pi - 2\theta_i)}{\cos\theta_i} e^{2iak_z^i}}{i\left\{\cos\theta_i + \left[\cos^2\theta_i + 2i\gamma S(0) - \frac{\gamma^2}{\cos^2\theta_i}(S(0)^2 - S_j(\pi - 2\theta_i)^2)\right]^{1/2}\right\} - \frac{\gamma S(0)}{\cos\theta_i}} \tag{6}$$

Here, the value of j is 1 for s polarization (TE) and 2 for p polarization (TM); the value of γ is the same as that in eq 1. Note the phase factor $e^{2iak_z^i}$ in the numerator. This factor arises from placing the first 2D sheet one radius away from the nominal surface for which the reflection coefficient is calculated. This factor was not included in the half-space reflection coefficients derived in ref 15 and later used in ref 16 because in those works, the nominal surface was taken to be the first 2D sheet and the phase factor was introduced later when considering an incident medium different from the matrix medium.

2.4. Extended Fresnel's Formulas: Heuristic Approximations. In this section, we review briefly the theoretical formalism used to calculate the reflection amplitudes from a turbid colloid, using the model described in section 2.1. Here, we do not divide the space occupied by the colloid into a periodic collection of slabs; we rather perform the averaging procedure in the whole half-space, and then discuss the complications that arise when one tries to extend effective-medium concepts to the reflection problem. We start by accepting the conclusions reached in ref 10, in relation to the nonlocal nature (spatial dispersion) of the bulk effective optical parameters of the colloid. Let us recall that spatial dispersion means that the optical response depends not only on the frequency of the incident plane wave but also on its wavevector. In ref 10, the effective optical response of the colloidal system is derived in terms of an effective nonlocal conductivity tensor $\bar{\bar{\sigma}}_{eff}(\vec{k}, \omega)$, which can be defined only within the effective-field approximation. This approximation assumes that the electromagnetic field exciting any of the particles is equal to the average field and is valid in general only in the dilute regime. The tensor $\bar{\bar{\sigma}}_{eff}(\vec{k}, \omega)$ relates linearly the (ensemble) average of the total current $\langle\vec{J}_{ind}\rangle$ induced in the spheres to the average of the electric field $\langle\vec{E}\rangle$ within the system, that is

$$\langle\vec{J}_{ind}\rangle(\vec{k}, \omega) = \bar{\bar{\sigma}}_{eff}(\vec{k}, \omega)\cdot\langle\vec{E}\rangle(\vec{k}, \omega) \tag{7}$$

Thus, it is some kind of generalized Ohm's law, where $\langle\vec{J}_{ind}\rangle(\vec{k}, \omega)$ and $\langle\vec{E}\rangle(\vec{k}, \omega)$ are the Fourier transforms of $\langle\vec{J}_{ind}\rangle(\vec{r}, t)$ and $\langle\vec{E}\rangle(\vec{r}, t)$ and $(\vec{k}, \omega)$ space. Here, $\langle\ldots\rangle$ denotes an average, while $(\vec{r}, t)$ denotes the position vector and time, respectively. In the mixed $(\vec{r}; \omega)$ space, eq 7 can be written as a convolution,

$$\langle\vec{J}_{ind}\rangle(\vec{r}, \omega) = \int \bar{\bar{\sigma}}_{eff}(|\vec{r} - \vec{r}'|; \omega)\cdot\langle\vec{E}\rangle(\vec{r}'; \omega)\, d^3r \tag{8}$$

that displays explicitly the spatial nonlocal nature of the response, as well as the on-the-average translational invariance and isotropy of the system. In $(\vec{k}, \omega)$ space, these properties imply that $\bar{\bar{\sigma}}_{eff}$ can be written as,

$$\bar{\bar{\sigma}}_{eff}(\vec{k}, \omega) = \sigma^L_{eff}(k, \omega)\hat{k}\hat{k} + \sigma^T_{eff}(k, \omega)(\bar{\bar{1}} - \hat{k}\hat{k}) \tag{9}$$

that is, in terms of only two scalar components, σ^L_{eff} and σ^T_{eff}, called the longitudinal and transverse components of $\bar{\bar{\sigma}}_{eff}$. In ref 10, how the two more traditional scalar optical responses $\epsilon_{eff}(\vec{k}, \omega)$ and $\mu_{eff}(\vec{k}, \omega)$ can be written in terms of $\sigma^L_{eff}(\vec{k}, \omega)$ and $\sigma^T_{eff}(\vec{k}, \omega)$ is also shown. This indicates that the colloidal system can have a magnetic response even if the inclusions are intrinsically nonmagnetic.

It is now quite immediate to see that the presence of an interface destroys the translational invariance of the system; thus, $\epsilon_{eff}(\vec{k}, \omega)$ and $\mu_{eff}(\vec{k}, \omega)$ cannot describe the optical response of the colloidal system with an interface. One way out is the use $\epsilon_{eff}(\vec{k}, \omega)$ and $\mu_{eff}(\vec{k}, \omega)$ together with the so-called additional boundary conditions (ABCs).[23] Unfortunately, this method works only in case the system has specific symmetry properties. In general, the presence of the interface modifies the optical response itself, that is, $\bar{\bar{\sigma}}_{eff}(|\vec{r} - \vec{r}'|; \omega) \to \bar{\bar{\sigma}}_{eff}(\vec{r}, \vec{r}'; \omega)$, being the modification stronger in a region close to the interface and depending also on its specific geometrical structure. Correspondingly, in $(\vec{k}, \omega)$ space, one has $\bar{\bar{\sigma}}_{eff}(\vec{k}, \omega) \to \bar{\bar{\sigma}}_{eff}(\vec{k}, \vec{k}'; \omega)$, and one chooses an interface as the one described in section 2.1.

At this point, one finds no advantage in calculating $\bar{\bar{\sigma}}_{eff}(\vec{k}, \vec{k}'; \omega)$ because there are no expressions in continuum electrodynamics[26] that link the reflection amplitudes to a quantity like $\bar{\bar{\sigma}}_{eff}(\vec{k}, \vec{k}'; \omega)$. Therefore, one has to go back to Maxwell's equations and tackle the problem right from the start without looking for an effective medium. This has been already done[18,19] by expressing the induced current in the system as the

DOI: 10.1021/acs.jpcb.5b10814
J. Phys. Chem. B 2016, 120, 583−595

sum of the currents induced at each sphere by an exciting field; the exciting field at each sphere is the field scattered by all other spheres but the one under consideration. The induced current at each sphere is expressed in terms of the nonlocal conductivity tensor of an isolated sphere, denoted by $\overline{\overline{\sigma}}_s(\vec{r}, \vec{r}'; \omega)$ in $(\vec{r}; \omega)$ space or $\overline{\overline{\sigma}}_s(\vec{k}, \vec{k}'; \omega)$ in $(\vec{k}; \omega)$ space, and the solution of Maxwell's equations leads to an integral equation that is solved using the effective-field approximation. In this approximation, one assumes that the exciting field at each sphere is given by the average field at that sphere; thus, it is valid only in the dilute regime. A plane-wave solution of the integral equation is found, and expressions for the reflection amplitudes for s- and p-polarization are also found, in terms of the components of $\overline{\overline{\sigma}}_s(\vec{k}^i, \vec{k}^r; \omega)$ and $\overline{\overline{\sigma}}_s(\vec{k}^i, \vec{k}^t; \omega)$. Here, $\vec{k}^i$, $\vec{k}^r$, and $\vec{k}^t$ denote the wavevector of the incident, reflected, and transmitted plane wave, respectively. It was also pointed out[19] that $\overline{\overline{\sigma}}_s(\vec{k}, \vec{k}'; \omega)$ is actually proportional to the T matrix of an isolated sphere, that is, the one used in scattering theory to describe the scattering properties of a sphere;[24] thus, this approach is indeed a multiple-scattering approach. Because the calculation of $\overline{\overline{\sigma}}_s(\vec{k}, \vec{k}'; \omega)$ is quite cumbersome, different approximations have been proposed[19] in terms of the scattering matrix of the isolated sphere.

Here, we will consider only the so-called HA,[19] where the reflection amplitudes are readily given by

$$r_s = \frac{S_1[\pi - (\theta_i + \theta_t)]}{S_1(\theta_i - \theta_t)} \frac{k_z^i - k_z^t}{k_z^i + k_z^t} e^{2iak_z^i} \tag{10}$$

$$r_p = \frac{S_2[\pi - (\theta_i + \theta_t)]}{S_2(\theta_i - \theta_t)} \frac{k_z^i - k_z^t}{k_z^i + k_z^t} e^{2iak_z^i} \tag{11}$$

where, as mentioned above, S_1 and S_2 are the diagonal elements of the scattering matrix, as defined in ref 8. Also note that in the numerators, the angle in the arguments of S_1 and S_2 is the angle between the direction of refraction and the direction of reflection, that is, the direction where the interference of the scattered field is always constructive. The phases in r_s and r_p come from the fact that the configurational average over the uncorrelated positions of the centers of the spheres covers a region of space that leaves out a slab of width a on the right-hand side of the nominal surface of the half-space. Here, $k_z^t(\omega)$ is obtained from the dispersion relation of the transverse modes given in terms of $\overline{\overline{\sigma}}_s(\vec{k}^t, \vec{k}^t; \omega)$; nevertheless, it was also shown[19] that a rather good approximation for $k_z^t(\omega)$ is given by $k_z^{eff}(\omega)$ as obtained from the Foldy–Lax dispersion relation,[20−22] that is

$$k_z^t = \sqrt{n_m^2 \cos^2\theta_t + \frac{3if}{(k_o n_m a)^3} S(0)} \tag{12}$$

and this is the value that will be used in our calculations. Here, n_m is the RI of the matrix of the colloid, and θ_t is the angle of refraction, and we recall that in deriving eqs 10 and 11, it is assumed that the incidence medium is the same as the matrix. Finally, the name heuristic comes because in performing an approximation for the components of $\overline{\overline{\sigma}}_s(\vec{k}^t, \vec{k}^t; \omega)$ and $\overline{\overline{\sigma}}_s(\vec{k}^i, \vec{k}^t; \omega)$, involved in the derived amplitude reflection coefficients,[19] in terms of the elements of the scattering matrix, the angles in the arguments did yield the correct small-particle limit only in the dilute regime, and they were modified "heuristically" in order to obtain the correct limit for denser systems.

2.5. Composition Formula for the Reflection Amplitudes. As will be seen below, our experimental arrangement measures the reflectivity from an interface between a glass prism and the colloidal suspension, explaining why we choose to model the interface as described in section 2.1, the glass being the nominal surface, but this requires also formulas for the reflection amplitudes for this interface. As mentioned earlier, the formulas for the CSM and the HA written above consider that the incidence medium and the matrix of the colloidal suspension are the same. Therefore, one still needs to find the corresponding formulas for the glass−colloid interface. For doing this, we use the well-known composition formula that relates the reflection amplitude at the interface between media 1 and 3 with the reflection amplitudes at the interfaces between media 1 and 2 and media 2 and 3, and it is given by[25]

$$r_{13} = \frac{r_{12} + r_{23}}{1 + r_{12}r_{23}} \tag{13}$$

In our case, medium 1 is glass, medium 2 is water, and medium 3 is the suspension of colloidal particles immersed in water (see Figure 3). Therefore, the formulas above for the

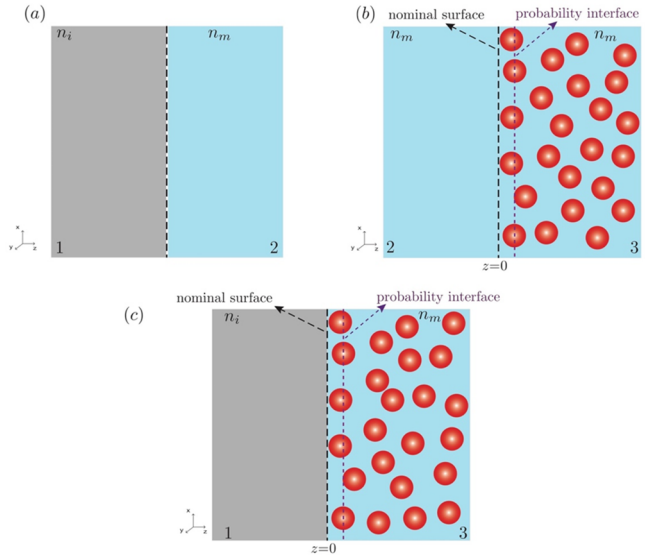

Figure 3. Sketches of the different cases being considered. (a) The incidence medium is different than the matrix. In this system, we have a glass−water interface. (b) The incidence medium is the same as the matrix medium, and the half-space of particles is thought of as an effective medium with an effective RI. (c) Half-space of randomly placed particles considering the that incidence medium is different than the matrix medium. The nominal surface and probability interfaces are indicated.

CSM and HA corresponds to r_{23}, while r_{12} is the reflection amplitude between glass and water, given by the standard Fresnel's formulas devised only in terms of the index of refraction of water and glass. If we now take as r_{23} eq 6 for CSM or eqs 10 and 11 for the HA and separate the phase explicitly by writing them as $r_{23} = \tilde{r}_{23}e^{2iak_{2z}}$ and then combine them with eq 12, one gets

$$r_{13} = \frac{r_{12} + \tilde{r}_{23}e^{2iak_{2z}}}{1 + r_{12}\tilde{r}_{23}e^{2iak_{2z}}} \tag{14}$$

where k_{2z} is the z component of the wavevector in water. One can readily see that this formula is the well-known formula for

DOI: 10.1021/acs.jpcb.5b10814
J. Phys. Chem. B 2016, 120, 583−595

the reflection amplitude for a three-layered system.[15] In other words, one can think that the reflection amplitude in our system, the glass-colloidal suspension, can be regarded as the reflection in a system composed of glass (medium 1), a small layer of water (medium 2), and the colloidal water suspension (medium 3). It is evident that the reflectivity will be dominated by the reflection at the glass−water interface, and this will show a critical angle whenever the index of refraction of the glass is larger than that of water. In this case, the reflectivity as a function of the angle of incidence shows a very sizable change before the critical angle, going to 1 at the critical angle. Now, if the water medium becomes a thin layer between the glass and the water suspension, the reflectivity, as a function of the angle of incidence, will lie between the one corresponding to the glass−water interface (layer of infinite length) and the one with a layer of size 0. This latter one corresponds to the simple 2MF approximation described in section 2.2. In our formalism, the size of the layer is equal to a, the radius of the spheres.

$$\tilde{r}_{23} = r_{23}e^{-2iak_{2z}} \tag{15}$$

2.6. Approximations. In sections 2.2−2.5, we explained three approximations that we can readily compare with experiments involving a monodisperse colloidal suspension. However, eq 15 allows us to construct one more approximation that is of interest here, namely, the 3-media Fresnel (3MF) approximation. Such an approximation follows naturally after noticing that the phase factor $e^{2iak_z^m}$ appearing in the reflection amplitudes corresponding to CSM (eq 6) and HA (eqs 10 and 11) comes from placing the nominal surface (for which the reflection coefficients are calculated) one radius away from the probability interface. This ensures that all particles are completely embedded in the matrix medium and do not penetrate the incidence medium. Similarly, we can improve the commonly used 2MF approximation by incorporating the phase factor $e^{2iak_z^m}$ to Fresnel's approximation given in eqs 3 and 4 above. In this way, the 3MF approximation takes into account the finite size of the particles, ensuring that they do not penetrate the incidence medium. Now, we can apply eq 13 to construct the reflection coefficient for the case when the incidence medium is different from the matrix. We get

$$r_{3MF} = \frac{r_{12} + r_{2MF}e^{2iak_{2z}}}{1 + r_{12}r_{2MF}e^{2iak_{2z}}} \tag{16}$$

where r_{2MF} is given either by eq 3 or 4, depending on the polarization of light, and of course, it yields r_{3MF} for that same polarization.

Summarizing, we will compare four approximations with the experimental data obtained in this work: (i) the 2MF approximation, (ii) the CSM, (iii) the HA, and (iv) the 3MF approximation. However, many colloids of practical interest are not monodisperse, and a particle size distribution must be taken into consideration. In the next section, we explain how to extend these four models to calculate the coherent reflectance from a polydisperse colloid.

2.7. Polydisperse Models. Many colloids of interest are polydisperse, meaning that particles have different radii a. Commonly, one can define a size distribution function $n(a)$ that is related to the probability density of finding a particle with radius between a and $a + da$. To be more specific, here let us assume that the particle size distribution is a log-normal distribution, commonly present in many samples of practical interest and given by

$$n(a) = \frac{1}{a\sqrt{2\pi}\,\ln(\sigma)}e^{-\log(a/a_o)^2/2\log(\sigma)^2} \tag{17}$$

where a_o is the most probable particle radius and σ is the width of the log-normal distribution. To take into account particle size polydispersity in the formulas given above, it is better to write them first in terms of the number density of particles, ρ, and not in terms of the volume fraction f.

For instance, considering the CSM in the case of a monodisperse system of particles of radius a with a particle number density of ρ, we can write eq 6 as

$$r_{hs} = \frac{\beta e^{2iak_z^i}}{i(k_z^{eff} + k_z^m) + \alpha} \tag{18}$$

where

$$\beta = -\frac{2\pi\rho}{k_m^2\cos(\theta_m)}S_j(\pi - 2\theta_m) \tag{19}$$

$$\alpha = -\frac{2\pi\rho}{k_m^2\cos(\theta_m)}S_j(0) \tag{20}$$

$$k_z^{eff} = \sqrt{(k_z^m)^2 - 2i\alpha k_z^m + \beta^2 - \alpha^2} \tag{21}$$

If we now consider a polydisperse system of particles, we must average the scattering coefficients β and α over the number density probability density function, $\rho(a)$. We have

$$\beta = -\frac{2\pi}{k_m^2\cos(\theta_m)}\int_0^\infty \rho(a)S_a(\pi - 2\theta_m)\,da \tag{22}$$

$$\alpha = -\frac{2\pi}{k_m^2\cos(\theta_m)}\int_0^\infty \rho(a)S_a(0)\,da \tag{23}$$

Notice that $k_m = k_o n_m$ and $\rho(a)$ using eq 17 is

$$\rho(a) = \frac{3f}{4\pi a_o^3}\left(\frac{1}{a\log\sqrt{2\pi}}\right)\exp\left[\frac{-\log\left(\frac{a}{a_o}\right)^2}{2\log(\sigma)^2}\right] \times \exp\left[\frac{-(3\log(\sigma))^2}{2}\right] \tag{24}$$

In the HA and both Fresnel approximations (2MF and 3MF), we should use the effective RI for a polydisperse colloid, given by

$$\tilde{n}_{eff} = n_m\left[1 + i\frac{2\pi}{k_m^3}\int_0^\infty \rho(a)S_a(0)\,da\right] \tag{25}$$

Additionally, the reflection amplitudes in the HA (eqs 10 and 11), where the ratio $S_j[\pi - (\theta_i + \theta_t)]/S_j[\theta_i - \theta_t]$ appears, should be replaced by

$$r_s = \frac{\beta_1}{\tau_1}\frac{k_z^i - k_z^t}{k_z^i + k_z^t}e^{2iak_z^i} \tag{26}$$

$$r_p = \frac{\beta_2}{\tau_2}\frac{k_z^i - k_z^t}{k_z^i + k_z^t}e^{2iak_z^i} \tag{27}$$

where

DOI: 10.1021/acs.jpcb.5b10814
J. Phys. Chem. B 2016, 120, 583−595

$$k_z^t = k_o\sqrt{n_m^2 - \frac{n_i^2}{n_m}\sin^2(\theta_i) + \int_0^\infty \rho(a)S_a(0)\,da} \tag{28}$$

$$\beta_j = \frac{3i}{k_m^3}\int_0^\infty \rho(a)S_{j,a}(\pi - \theta_i - \theta_t)\,da \tag{29}$$

$$\tau_j = \frac{3i}{k_m^3}\int_0^\infty \rho(a)S_{j,a}(\theta_i - \theta_t)\,da \tag{30}$$

where j takes values 1 or 2 for s or p polarization, respectively.

However, there is an additional complication to construct the half-space reflection coefficient for polydisperse colloids. Because particles cannot penetrate the incidence medium, it is no longer possible to define a probability interface in the way that we did for a monodisperse system of particles because the centers of smaller particles can approach closer the nominal surface than the centers of larger particles. It is possible to subdivide a region of finite width near the nominal surface into thin slabs with the corresponding particle size distribution for each slab and then solve for the reflectance of the system using an iterative procedure. This was explored in ref 27 using the CSM. It was found that for log-normal size distributions with a width parameter σ smaller than 2, in the case of latex particles in water, one can use a simple approximation referred to as the "sharp-surface approximation", with negligible error. For TiO_2 particles in water, the differences between the sharp-surface approximation and the iterative procedure were clearly noticeable only for σ = 1.6. The sharp-surface approximation consists of replacing the particle radius, appearing in the phase factor $e^{2iak_z^m}$ in the formulas for the monodisperse case, with the most probable radius. That is, for a polydisperse colloid, we substitute

$$\exp(2ik_z^m a) \rightarrow \exp(2ik_z^m a_o) \tag{31}$$

in the half-space reflection coefficients given in eqs 6, 10, and 11 and then use the resulting reflection coefficient in eq 15. The same replacement is done in eq 16 for the 3MF approximation with a polydisperse colloid.

3. EXPERIMENTAL SETUP

As already mentioned, the highest sensitivity to the presence of the colloidal particles in reflectance measurements from a colloidal half-space is for angles of incidence around the critical angle in an internal reflection configuration. Our objective here is to estimate the validity limits of the available theoretical models presented in section 2 around the critical angle for common colloidal suspensions. Thus, we devised a fast and versatile experimental setup to measure the reflectivity as a function of incidence angle in a small-angle range around the critical angle.

Our experimental device is illustrated in Figure 4 and is based in the experimental setup developed in ref 28. It consists of a semicircular prism made of BK7 glass of 3 cm of radius, a concave-plane prism also of BK7 glass, a dynamic diffuser, a polarizer, two convex lenses, and a CCD camera (Thorlabs DCC1545M model). The two lenses have focal lengths of 6 (lens 1) and 3.5 cm (lens 2). We use two diodes lasers with 405 and 638 nm wavelengths. The container is made of two pieces; one is a short iron cylinder glued to the base of the prism with its external surface threaded, and the second one is a Teflon lid that screws around the iron piece, forming a sealed container that can hold liquids in contact with the base of the optical

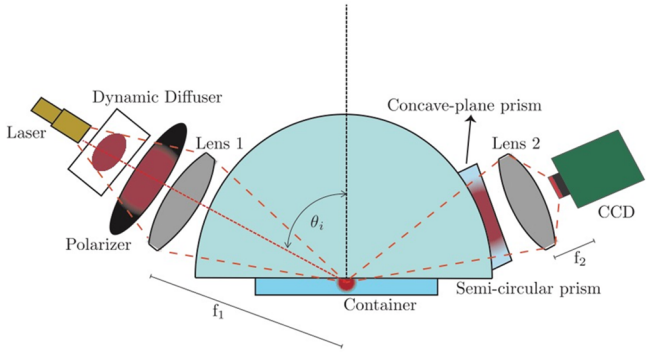

Figure 4. Experimental setup to measure the coherent reflectance of light as a function of the angle of incidence in an internal reflection configuration around the critical angle of the glass–water interfaces.

prism. The laser beam is scattered by the diffuser, and the first lens (lens 1 in the Figure 4) collects and focuses the scattered light at the base of the prism and in the center of the interface with the container. The optical axis of the focused light makes an angle of incidence at the base of the prism equal to the critical angle of a BK7 glass–water interface. The optical axis of the reflected light exits the semicircular prism and passes through the centers of the concave-plane prism and lens 2. The concave-plane prism is used to reduce the defocusing of the reflected beam due to the curved surface of the semicircular prism, and the convex lens 2 is used to map the angular distribution of coherent reflected light to a spatial distribution at the focal plane of lens 2. The CCD camera is placed at the focal distance from lens 2 to register the spatial distribution on the intensity of reflected light.

The polarizer is rotated to choose the polarization of the incident light (s or p). The diffuser used to scatter light previous to being focused is rotated at constant speed to average out the speckle on the CCD image. Also, the image at the CCD is integrated in the direction perpendicular to the plane of incidence (the plane of the drawing in Figure 4) to reduce further speckle noise. The resulting one-dimensional intensity map gives the angular intensity profile of light exiting the prism simply by translating a linear step toward the center of the CCD along the plane of incidence to steps in the angle of travel of light inside of the semicircular prism. This is done using simple geometrical optics.[28] The angular range captured by the CCD corresponds to a 6° angle of travel inside of the semicircular prism.

When the sample chamber is filled with a turbid sample, in addition to light reflected from the prism–sample interface, some diffuse light scattered with the turbid sample will reach the detection plane of the CCD. However, the amount of diffuse light reaching the CCD is negligible compared to the coherently reflected light at the interface and is simply ignored.

4. EXPERIMENTAL PROCEDURE

The angular intensity profile measured at the focal plane of lens 2 for a given liquid sample is converted to a reflectivity curve dividing the sample intensity profile by the one obtained with the container empty (actually, filled with air). The latter profile corresponds when there is total internal reflection at the base of the prism for all angles of incidence captured by the CCD and thus to a unit reflectance at all angles of incidence. For instance, the reflectivity curve for water is obtained as

DOI: 10.1021/acs.jpcb.5b10814
J. Phys. Chem. B 2016, 120, 583–595

$$R_{water} = \frac{I_{glass-water}}{I_{glass-air}} \quad (32)$$

where $I_{glass-air}$ and $I_{glass-water}$ are the intensity profiles measured with the container filled with water and air, respectively.

In addition to the angular step size in the reflectivity profiles obtained with the CCD, which as already said is obtained from geometrical considerations, to calibrate the angular scale of the reflectivity curves, we need to identify the exact value of one angle of incidence in the angular scale of the intensity profiles. To do this, we obtain the reflectivity curve for tridistilled water, identify the critical angle from the intensity profile, and assign to it the value calculated from Snell's law and tabulated values of the refractive indices of tridistilled water and BK7 glass at the corresponding wavelength.[29,30] We identify the critical angle as the inflection point of the reflectivity curve.

In Figure 5, we plot the reflectivity profile obtained by our system for tridistilled water and the theoretical curve of the plane-wave reflectance at a BK7 glass−tridistilled water interface. The calibrated angular scale is already shown.

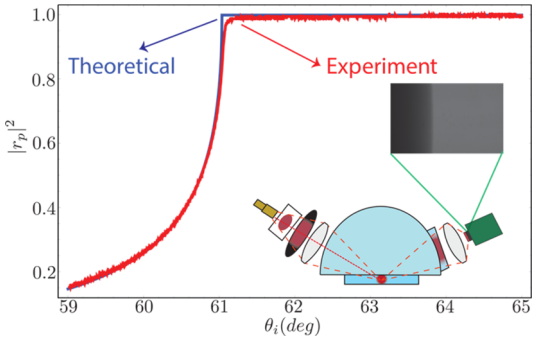

Figure 5. Experimental reflectance as a function of the angle of incidence around the critical and the theoretical plane-wave reflectance of the BK7 glass−water interface, using a wavelength of 405 nm.

We can appreciate that there is a smoothing of the experimental profile just around the critical angle in comparison with the theoretical curve. The reason is that the experimental curve is not for a plane wave. It is not difficult to see that each point in the experimental curve actually corresponds to an average of the plane-wave reflectance over a small angular range due to the finite lateral extent of the CCD pixels.

We prepared turbid colloidal suspensions of nanoparticles of poly(methyl methacrylate) (PMMA) particles of diameters 120 and 520 nm, TiO_2 (rutile) with a 404 nm most probable diameter, and copper particles of 500 nm average diameter in tridistilled water. The latex and copper particles were spherical according to the manufacturers, whereas the TiO_2 particles were irregular shapes but spheroidal on average, as seen by transmission electron micrographs. The polydispersity index of the PMMA particles around 1.02 (measured by dynamic light scattering) and can be considered monodisperse. The TiO_2 particles are polydisperse with a log-normal size distribution with an estimated width parameter of about 1.3.[31] The copper nanoparticles are polydisperse, but the manufacturer did not provide information about their size distribution. Thus, we consider them here as monodisperse with the average diameter reported by the manufacturer.

For the numerical calculations, we need the RI of each type of particle. The RI of the particles was obtained from tables.[32−34] For PMMA particles, the RI that we used was 1.51 for the 405 nm wavelength and 1.49 for the 638 nm wavelength. The RI of TiO_2 (rutile) particles that we used was 3.37 + 0.097i for the 405 nm wavelength and 2.58 for 638 nm, and for particles of copper, the RI for the 638 nm wavelength that we used was 0.29 + 3.49i. We prepared colloidal suspensions of PMMA particles of 120 nm diameter with the following filling fractions: 3.0, 15.4, 18.5, and 24.1%. For latex suspensions of 520 nm in diameter, we used the following filling fractions: 1.7, 1.9, 4.0, and 6.0%. The suspensions of TiO_2 had volume concentrations of 0.1, 0.2, 0.8, and 1.1%, and the colloidal suspensions of copper were prepared at only two volume concentrations, 0.1 and 0.2%.

The stability of the colloidal suspensions is an important prerequisite for our study; therefore, we monitored the reflectivity over time of all of the prepared suspensions, prior to measuring the nominal curve for its comparison with theory.[35] Before measuring any sample, this was sonicated for

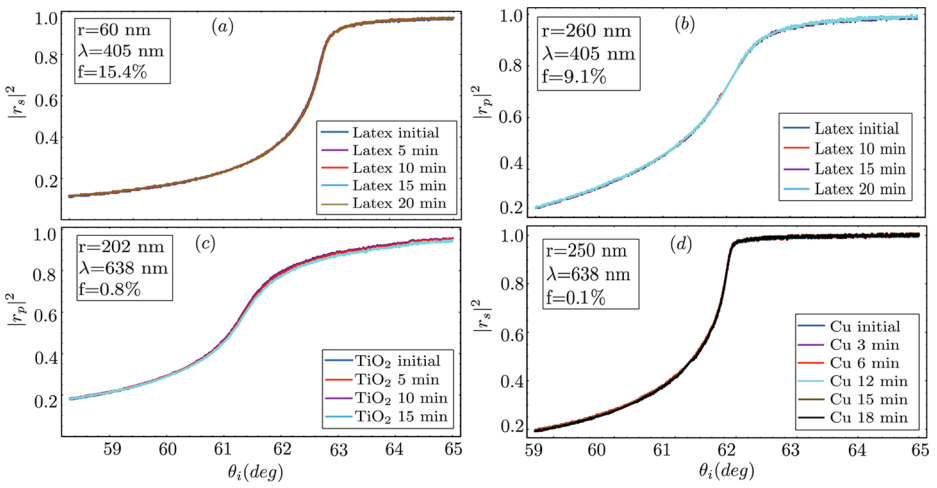

Figure 6. Experimental reflectance as a function of the angle of incidence around the critical angle at different times. (a) Reflectance of a colloidal suspension of 120 nm diameter PMMA particles at a wavelength of 405 nm. (b) Reflectance of a colloidal suspension of 520 nm diameter PMMA particles at a wavelength of 405 nm. (c) Reflectance of a colloidal suspension of 404 nm diameter TiO_2 particles at a wavelength of 638 nm. (d) Reflectance of a colloidal suspension of 500 nm diameter copper particles at a wavelength of 638 nm.

DOI: 10.1021/acs.jpcb.5b10814
J. Phys. Chem. B 2016, 120, 583−595

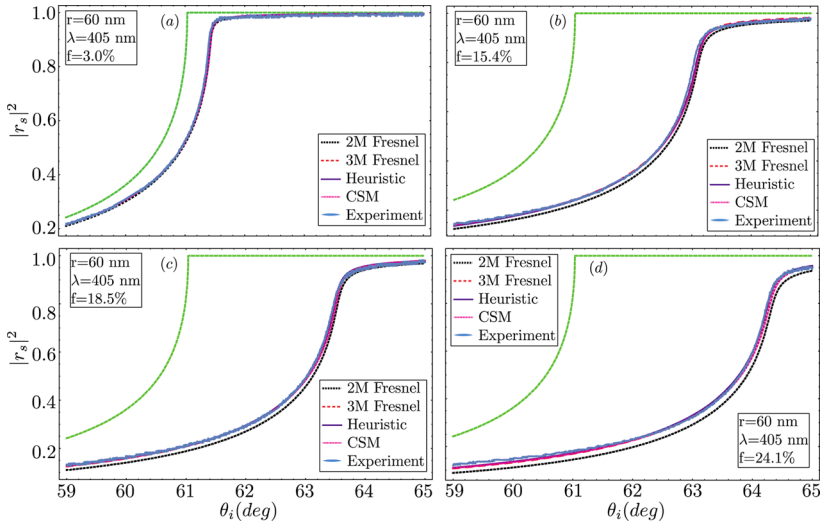

Figure 7. Experimental reflectance as a function of the angle of incidence around the critical angle and theoretical predictions for colloidal suspensions of 120 nm diameter PMMA particles, using 405 nm laser light wavelength and different volume filling fractions: (a) 3.0, (b) 15.4, (c) 18.5, and (d) 24.1%. The green dashed curve is the reflectance curve for pure water. The polarization of light is indicated by the subscript on the ordinate axis label (s polarization).

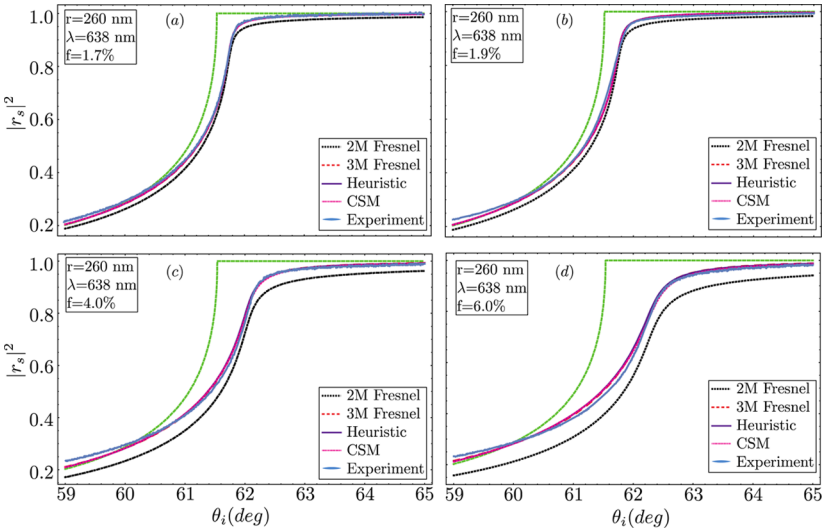

Figure 8. Experimental reflectance as a function of the angle of incidence around the critical angle and theoretical predictions for colloidal suspensions of 520 nm diameter PMMA particles, using laser light of 638 nm wavelength and different volume filling fractions: (a) 1.7, (b) 1.9, (c) 4.0, and (d) 6.0%. The green dashed curve is the reflectance curve for pure water. The polarization of light is indicated by the subscript on the ordinate axis label (s polarization).

about 5 min in an ultrasonic bath (Branson 200) in order to break any aggregates that might have formed and then introduced in the container. In Figure 6, we present reflectance curves around the critical angle taken at different times during a period of 15 or 20 min. We can appreciate in the plots of Figure 6 that these remain constant during the lapse of time in which they were observed. This indicated that the particles were well-dispersed and stable in suspension, at least for that lapse of time. Only in Figure 6c can we appreciate a slight difference between the initial measurements and those after 15 min. However, the difference is less than 0.1%. On the other hand, obtaining a reflectivity curve for any sample after it had been sonicated took less than 2 min.

We measured the reflectance curves around the critical angle for s and p polarization for all of the suspensions prepared at the two available wavelengths, 638 and 405 nm, and compared with theoretical predictions.

5. THEORY–EXPERIMENT COMPARISON AROUND THE CRITICAL ANGLE

In this section, we compare the theoretical predictions by the models presented in section 2 with experimental reflectivity curves around the critical angle obtained for the different turbid colloidal suspensions that we prepared and described in section 4. In Figures 7–9, we present the results for the 120 and 520 nm diameter PMMA (latex) samples and for different concentrations prepared and either s- or p-polarized light (indicated in the subscript on the label for the ordinate axis).

In Figure 7a, there are no appreciable differences between any of the theoretical predictions and the experiment. Even the 2MF approximation reproduces very well the experimental

DOI: 10.1021/acs.jpcb.5b10814
J. Phys. Chem. B 2016, 120, 583–595

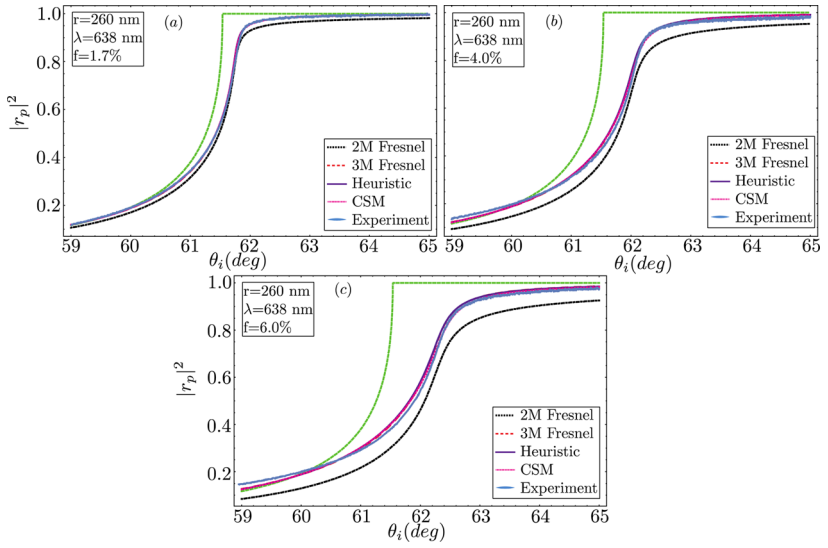

Figure 9. Experimental reflectance as a function of the angle of incidence around the critical angle. Comparing the theoretical models with the experiments. Colloidal suspensions of 520 nm diameter latex (PMMA), using a light source of 638 nm wavelength at different filling fractions: (a) 1.7, (b) 4.0, and (c) 6.0%. The green dashed curve is the reference of the prism−water interface.

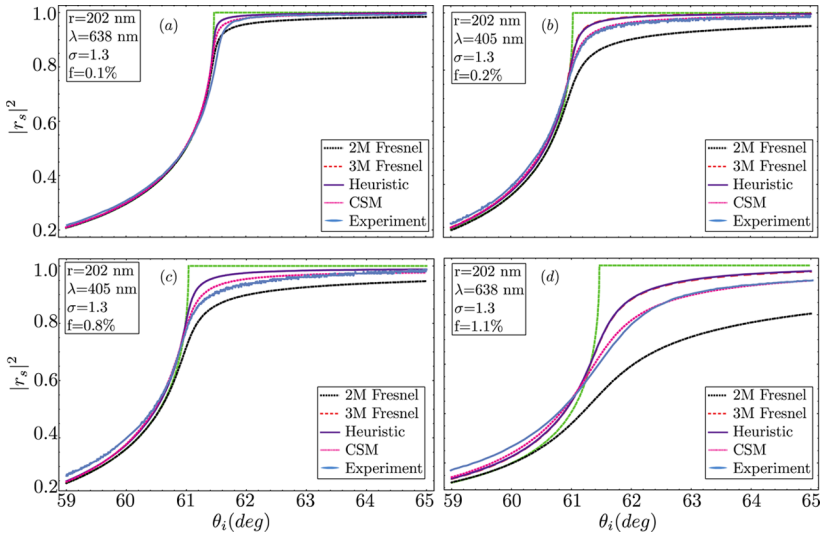

Figure 10. Experimental reflectance as a function of the angle of incidence around the critical angle for s-polarized laser light of 638 nm vacuum wavelength (a,d) and laser light of 405 nm vacuum wavelength (b,c) and theoretical predictions for suspensions of titanium dioxide (rutile) particles. The most probable particle diameter is 404 nm, and the width parameter was assumed to be 1.3. The particles' volume filling fractions are (a) 0.1, (b) 0.2, (c) 0.8, and (d) 1.1%. The green dashed curve is the reflectance curve for pure water.

data. In Figure 7b−d, the HA and 3MF approximation follow closely the experimental curve, whereas the CSM deviates slightly, and the 2MF deviates noticeably. Thus, we conclude that for small particles (less than 120 nm of diameter) and small concentrations (less than about f = 3%), any of the four models can be used around the critical angle with very good precision. For small particles and higher concentration, the HA and 3MF remain very good approximations up to 24% of the particles' volume concentration.

In Figure 8, we can see that the HA, 3MF, and the CSM reproduce well the experimental data, whereas the predictions by the 2MF approximation differ noticeably in all cases (more for the higher concentration). For 6.0% of the particles' volume fraction, the difference between the experiment and the 2MF is about 20% and higher for all angles of incidence shown. The same results were obtained for p polarization, as shown in Figure 9.

In Figure 10, we present the results for polydisperse suspensions of titanium dioxide particles. We show results for s-polarized light of 405 nm vacuum wavelength only. The theoretical predictions were calculated assuming a log-normal size distribution with a most probable diameter of 404 nm and a width parameter of σ = 1.3.[31] In these cases, we can appreciate that the HA and 3MF nearly coincide with each other and deviate somewhat from the experimental curves (5% or less). The difference is more noticeable for angles of incidence close to and larger than the critical angle for water, whereas the CSM reproduces the experimental data better for all of the particles' volume fractions considered. The 2MF approximation differs significantly from the experimental curves. The difference is larger for higher particle concen-

DOI: 10.1021/acs.jpcb.5b10814
J. Phys. Chem. B 2016, 120, 583−595

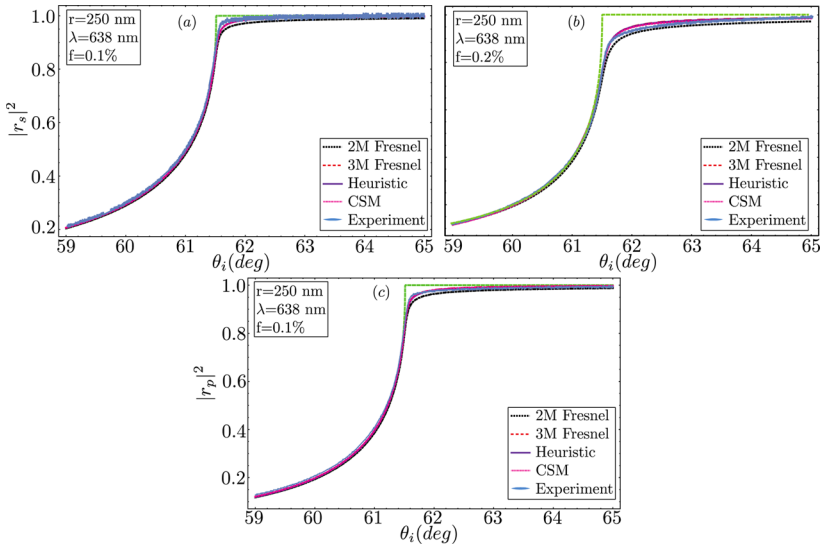

Figure 11. Experimental reflectance as a function of the angle of incidence around the critical angle at different filling fractions of colloidal suspensions of copper particles with 500 nm diameter and theoretical predictions. The wavelength of light is 638 nm. The polarization of light and the volume filling fractions are s polarization and $f = 0.1$ and 0.2% for (a) and (b) respectively and p polarization and $f = 0.1\%$ for part (c). The green dashed curve is the reference of the prism−water interface.

trations, reaching the highest difference of 15% for the most concentrated sample with $f = 1.1\%$ and for the highest angle of incidence of about 65°. These results suggest that for highly scattering particles, the CSM is the most precise model among those considered in this paper.

The results for suspensions of copper particles with p-polarized light and an incident wavelength of 638 nm are displayed in Figure 11. Both cases shown are for very dilute samples (0.1 and 0.2%). As said before, to compute the theoretical predictions, we assumed that the particles were monodisperse with a diameter equal to that stated by the manufacturer (500 nm). We can appreciate that the HA, the 3MF, and the CSM agree well with the experimental curves. The 2MF differs noticeably for angles of incidence near the glass−water critical angle and larger angles of incidence (up to a 3% difference).

The comparisons of the theoretical predictions by the four models considered in this work and the experimental data obtained for both light polarization (p or s) and the wavelength of light (405 or 638 nm), which are not shown in Figures 7−11, revealed the same trends observed in these figures.

6. SUMMARY AND CONCLUSIONS

Our objective in this work was to compare available theoretical models for the coherent reflectance from a colloidal half-space with experimental results without performing any fit of the parameters involved in order to obtain a reliable idea about their validity.

We obtained plots of the reflectivity measurements versus the angle of incidence with laser light having wavelengths of 638 and 405 nm for a set of colloidal suspensions in an internal reflection configuration around the critical angle. Then, we compared the experimental results with predictions by four different models. The samples consisted of latex spherical particles made of PMMA with a RI of 1.49 and 1.51 (at 638 and 405 nm wavelengths, respectively) and TiO_2 (rutile) particles with a RI of 2.58 and 3.37 + 0.097i (at 638 and 405 nm wavelengths, respectively). We also included two curves for very dilute suspensions of copper particles with a RI of 0.29 + 3.49i (at a 638 nm wavelength), for which we only knew the most probable radius. The incidence medium was a BK7 optical glass, and the reflectivity measurements spanned 6° in angles of incidence around the critical angle. The latex colloids were monodisperse of two different diameters, 120 and 520 nm, whereas the suspensions of TiO_2 were polydisperse with a log-normal size distribution, with a most probable radius of 202 nm and a width parameter of about 1.3. For each type of colloidal suspension, we obtained reflectivity measurements for four different volume concentrations of particles. For the latex particles 120 and 520 nm in diameter, the maximum concentrations were 24.1 and 6.0%, respectively. For the suspensions of TiO_2, the maximum concentration was 1.1%. The suspensions of copper were of particles with an average diameter of 500 nm suspended in water and with concentrations of 0.1 and 0.2%.

The models considered for their comparison with the experimental data were briefly described and discussed in the text, and they were labeled as 2MF, 3MF, HA, and CSM.

The experiment−theory comparison showed that for the 120 nm particle diameter latex colloids, all models considered approximated well the experimental curves for the most diluted sample with a 3% volume concentration. For denser colloids, the curves predicted by the 2MF model deviated noticeably from the experimental data in all cases. The deviations of the 2MF predictions from the experimental curves are larger the higher the particle volume concentration, size, and RI.

The other three models reproduce quite well the experimental curves in all cases considered. The results presented in section 5 propose that the HA is slightly better for smaller particles (less strongly scattering particles) and can go to higher particle volume densities than the CSM, whereas the CSM is somewhat better for highly scattering particles and can reproduce well curves where the presence of the particles drops the reflectance by as much as 50% down from total reflectance (by this, we mean that the reflectance would have been unity in the absence of the particles). We must note that the CSM had already been tested against experimental data in ref 16, finding similar results.

DOI: 10.1021/acs.jpcb.5b10814
J. Phys. Chem. B 2016, 120, 583−595

It is surprising that the 3MF approximation is very close to the HA in all cases considered in the experiments, performing well in all cases although better for smaller particles. Notice that both approximations, 3MF and 2MF, are indeed effective-medium theories because both of them regard the colloid as homogeneous with an effective index of refraction. The only difference between them is that 3MF considers that there is a small gap of water between the glass and the colloid, while for 2MF, this gap is absent. The fact that for large particles and moderate filling fractions 2MF deviates pronouncedly from the experimental data while 3MF follows closely the HA clearly means that for angles of incidence in the neighborhood of the critical angle, the presence of the gap of water plays a very prominent role. This close resemblance between 3MF and the HA does not hold in general at lower angles of incidence.[19]

It is also startling the fact that the 3MF approximation performs very well for the smaller latex particles of 120 nm diameter even at concentrations as high as 24%. The reason this might be unanticipated is that we used the 3MF with the effective RI given in eq 1, while it is known that even for small particles and moderate filling fractions, the imaginary part of the effective RI does not follow eq 1 (ref 36 and references therein). This means that the real part of the effective RI plays a crucial role in how light reflects around the critical angle, whereas the sensitivity of the reflectance to the imaginary part of the effective RI around the critical angle is very much reduced. This conclusion supports the idea that the real part of the effective RI can in fact be determined accurately from measurements of reflectance in the neighborhood of the critical angle, as has been proposed in the past.[11,14,37]

We must point out however that numerical evaluation of the models considered in this paper shows that the relative differences between them can be much larger at smaller angles of incidence for particles of sizes comparable with the wavelength of radiation, and this means that the Fresnel coefficients can be worse than a simple rough approximation. The reason is that in Fresnel's approximations, only the forward-scattering amplitude of the particles, $S(0)$, is involved, whereas in the HA and CSM models, also the coefficients of the amplitude scattering matrix S_1 or S_2 evaluated in the specular direction $(\pi - 2\theta_i)$ are involved. These latter coefficients may differ strongly from $S(0)$ for small angles of incidence.

AUTHOR INFORMATION

Corresponding Author

*E-mail: augusto.garcia@ccadet.unam.mx.

Notes

The authors declare no competing financial interest.

ACKNOWLEDGMENTS

We want to acknowledge gratefully financial support from Dirección General de Asuntos del Personal Académico from Universidad Nacional Autónoma de México through Grants PAPIIT IN 1006015 and PAPIIT IN 113815. G.M.-L. and H.C.-T. are grateful for a CONACyT/UNAM scholarship supporting their graduate studies. Finally, we are also grateful to Dr. Asur Guadarrama for technical support in the laboratory during the course of this work.

REFERENCES

(1) Landauer, R. Electrical Conductivity in Inhomogeneous Media. *Proceedings of the First Conference on Electrical Transport and Optical Properties of Inhomogeneous Media*; Garland, J. C., Tanner, D. B., Eds.; American Institute of Physics: Woodbury, NY, 1978; Vol. *40*, pp 2−45.

(2) Gubernatis, J. E. Scattering Theory and Effective Medium Approximation to Heterogeneous Materials. *Proceedings of the First Conference on Electrical Transport and Optical Properties of Inhomogeneous Media*; Garland, J. C., Tanner, D. B., Eds.; American Institute of Physics: Woodbury, NY, 1978; Vol. *40*, pp 84−97.

(3) Rayleigh, L. On the Transmission of Light Through an Atmosphere Containing Small Particles in Suspension, and on the Origin of the Blue of the Sky. *Philos. Mag.* **1899**, *47*, 375−384.

(4) Garnett, J. C. M. Colours in Metal Glasses and in Metallic Films. *Philos. Trans. R. Soc., A* **1904**, *203*, 385−420.

(5) Fuchs, R. Optical Properties of Small Particles Composites. *Proceedings of the First Conference on Electrical Transport and Optical Properties of Inhomogeneous Media*; Garland, J. C., Tanner, D. B., Eds.; American Institute of Physics: Woodbury, NY, 1978; Vol. *40*, pp 276−281.

(6) Tsang, L.; Kong, J.; Ding, A. K-H. *Scattering of Electromagnetic Waves: Advanced Topics*; John Wiley: New York, 2001; Vol. *3*.

(7) Hulst, H. C. *Light Scattering by Small Particles*; Dover Publications: New York, 1981.

(8) Bohren, C. F.; Huffman, D. R. *Absorption and Scattering of Light by Small Particles*; John Wiley and Sons: New York, 1983.

(9) Mie, G. Contributions to the Optics of the Turbid Media Particularly of Colloidal Metal Solutions. *Ann. Phys.* **1908**, *330*, 377−445.

(10) Barrera, R. G.; Reyes-Coronado, A.; García-Valenzuela, A. Nonlocal Nature of the Electrodynamic Response of Colloidal System. *Phys. Rev. B: Condens. Matter Mater. Phys.* **2007**, *75*, 184202.

(11) García-Valenzuela, A.; Sánchez-Pérez, C.; Barrera, R. G.; Reyes-Coronado, A. Surface Effects on the Coherent Reflection of Light from a Polydisperse Colloid. Progress in electromagnetics research symposium, Hangzhou, China, 2005; pp 22−26.

(12) Mohammadi, M. Colloidal Refractometry: Meaning and Measurement of Refractive Index of Dispersions; The Science that Time Forgot. *Adv. Colloid Interface Sci.* **1995**, *62*, 17−29.

(13) Meeten, G. H.; North, A. N. Refractive Index Measurement of Absorbing and Turbid Fluids by Reflection Near the Critical Angle. *Meas. Sci. Technol.* **1995**, *6*, 214−221.

(14) Meeten, G. H.; North, A. N. Refractive index measurement of turbid colloidal fluids by transmission near the critical angle. *Meas. Sci. Technol.* **1991**, *2*, 441−447.

(15) Barrera, R. G.; García-Valenzuela, A. Coherent Reflectance in a System of Random Mie Scatterers and its Relation to the Effective-Medium Approach. *J. Opt. Soc. Am. A* **2003**, *20*, 296−311.

(16) García-Valenzuela, A.; Barrera, R. G.; Sánchez-Pérez, C.; Reyes-Coronado, A.; Méndez, E. R. Coherent Reflection of Light from a Turbid Suspension of Particles in an Internal-Reflection Configuration: Theory Versus Experiment. *Opt. Express* **2005**, *13*, 6723.

(17) García-Valenzuela, A.; Gutiérrez-Reyes, E.; Barrera, R. G. Multiple-Scattering Model for the Coherent Reflection and Transmission of Light from a Disordered Monolayer of Particles. *J. Opt. Soc. Am. A* **2012**, *29*, 1161.

(18) Gutierrez-Reyes, E. Reflexión de la luz por un semiespacio de esferas desordenadas. Ph.D. Thesis, Universidad Nacional Autónoma de México, Distrito Feredal, August 2013.

(19) Gutierrez-Reyes, E.; García-Valenzuela, A.; Barrera, R. G. Extension of Fresnel's Formulas for Turbid Colloidal Suspension: A Rigorous Treatment. *J. Phys. Chem. B* **2014**, *118*, 6015−6031.

(20) Foldy, L. L. The Multiple Scattering Waves. *Phys. Rev.* **1945**, *67*, 107−119.

(21) Lax, M. Multiple Scattering Waves. *Rev. Mod. Phys.* **1951**, *23*, 287−310.

(22) Lax, M. Multiple Scattering Waves II. The Effective Field in Dense Systems. *Phys. Rev.* **1952**, *85*, 621−629.

(23) Fuchs, R. Optical Properties of Small Particle Composites. *Proceedings of the First Conference on Electrical Transport and Optical Properties of Inhomogeneous Media*; Garland, J. C., Tanner, D. B., Eds.;

DOI: 10.1021/acs.jpcb.5b10814
J. Phys. Chem. B 2016, 120, 583−595

American Institute of Physics: Woodbury, NY, 1978, Vol. *40*, pp 276−281.
(24) Tsang, L.; Kong, J. A. Effective Propagation Constants for Coherent Electromagnetic Waves Propagating in Media Embedded with Dielectric Scatters. *J. Appl. Phys.* **1982**, *53*, 7162−7173.
(25) Landau, L. D.; Lifshitz, E. M. *Electrodinámica de Medios Continuos*; Fizmatgiz, Moscú: Madrid, 1981; Vol. *8*.
(26) Jackson, J. D.; *Classical Electrodynamics*; 2nd ed.; John Wiley and Sons, Inc.: New York, 1925.
(27) García-Valenzuela, A.; Sánchez-Pérez, C.; Barrera Perez, R. G.; Reyes-Coronado, A. Surface Effects on the Coherent Reflection of Light from a Polydisperse Colloid. *PIERS Online* **2005**, *1*, 650.
(28) Contreras-Tello, H.; García-Valenzuela, A. Refractive Index Measurement of Turbid Media by Transmission of Backscattered Light Near the Critical Angle. *Appl. Opt.* **2014**, *53*, 4768.
(29) Hale, G. M.; Querry, M. R. Optical Constants of Water in the 200-nm to 200-μm Wavelength Region. *Appl. Opt.* **1973**, *12*, 555−563.
(30) Schott optical glass data sheets, 2012-12-04.
(31) Curiel-Villasana, F. A. Predicción de propiedades ópticas de películas inhomogéneas por medio de modelos de transferencia radiativa y su aplicación en pinturas. Ph. D. Thesis, Universidad Nacional Autónoma de México, Distrito Federal, May 2004.
(32) Sultanova, N.; Kasarova, S.; Nikolov, I. Dispersion Properties of Optical Polymers. *Acta Phys. Pol., A* **2009**, *116*, 585−587.
(33) Devore, J. R. Refractive Indices of Rutile and Sphalerite. *J. Opt. Soc. Am.* **1951**, *41*, 416−419.
(34) Rakic, A. D.; Djurisic, A. B.; Elazar, J. M.; Majewski, M. L. Optical Properties of Metallic Films for Vertical-Cavity Optoelectronic Devices. *Appl. Opt.* **1998**, *37*, 5271−5283.
(35) Morales-Luna, G. Reflectividad de coloides turbios: Teoría-Experimento. M. Sc. Thesis, Universidad Nacional Autónoma de México, Distrito Federal, August 2015.
(36) García-Valenzuela, A.; Contreras-Tello, H.; Olivares, J. A.; Cuppo, F. L. S. Insights into the Dependent-Scattering Contributions to the Extinction Coefficients in Highly Scattering Suspensions. *J. Opt. Soc. Am. A* **2013**, *30*, 1328.
(37) Calhoun, W. R.; Maeta, H.; Combs, A.; Bali, L. M.; Bali, S. Measurement of the Refractive Index of Highly Turbid Media. *Opt. Lett.* **2010**, *35*, 1224.

DOI: 10.1021/acs.jpcb.5b10814
J. Phys. Chem. B 2016, 120, 583−595